Non-Rigid Groupwise Registration for Motion Estimation and Compensation in Compressed Sensing Reconstruction of Breath-Hold Cardiac Cine MRI

Authors

Javier Royuela-del-Val[1], Lucilio Cordero-Grande[2], Federico Simmross-Wattenberg[1], Marcos Martín-Fernández and Carlos Alberola-López[1]

[1]Universidad de Valladolid, Valladolid, Spain

[2]King's College London, London, UK

Corresponding Author:

Javier Royuela-del-Val,

Image Processing Laboratory

University of Valladolid

ETSI Telecomunicación, Campus Miguel Delibes s.n.

47011 Valladolid, Spain.

Email: jroyval@lpi.tel.uva.es

Phone: +34 983 423660, ext. 5590

Keywords: dynamic MRI reconstruction, compressive sensing, groupwise registration

Word count: 4937

Abstract

Purpose: Compressed sensing methods with motion estimation and compensation techniques have been proposed for the reconstruction of accelerated dynamic MRI. However, artifacts that naturally arise in compressed sensing reconstruction procedures hinder the estimation of motion from reconstructed images, especially at high acceleration factors. This work introduces a robust groupwise non-rigid motion estimation technique applied to the compressed sensing reconstruction of dynamic cardiac cine MRI sequences.

Theory and Methods: A spatio-temporal regularized, groupwise, non-rigid registration method based on a B-splines deformation model and a least squares metric is used to estimate and to compensate the movement of the heart in breath-hold cine acquisitions and to obtain a quasi-static sequence with highly sparse representation in temporally transformed domains.

Results: Short axis in vivo datasets are used for validation, both original multi-coil as well as DICOM data. Fully sampled data were retrospectively undersampled with various acceleration factors and reconstructions were compared with the two well-known methods k-t FOCUSS and MASTeR. The proposed method achieves higher signal to error ratio and structure similarity index for medium to high acceleration factors.

Conclusions: Reconstruction methods based on groupwise registration show higher quality reconstructions for cardiac cine images than the pairwise counterparts tested.

Introduction

Breath-hold (BH) cardiac cine MRI has become the gold standard for myocardial function imaging (1). In patients with diminished BH capacity this approach results in substantially compromised image quality (2). A respiratory-navigated, free-breathing examination can be performed as an alternative that, however, can result in unpredictably long acquisition times. Shortening the needed acquisition time can enable some of these patients to get a regular BH scan and, generally speaking: 1) improves patient comfort and reduces stress, 2) significantly reduces exam duration and the associated economical costs. Therefore, the development of faster acquisition methods is of great importance.

Reduced-data imaging methods take advantage of redundancy in the images to recover the whole image from only a fraction of the k-space data, shortening acquisition time consequently. In classical approaches, such as k-t BLAST/SENSE (3) and k-t GRAPPA (4), data are acquired

following a regular pattern and the spatio-temporal correlation is exploited to recover the original image. More recently, compressive sensing (CS) theory (5, 6) has been successfully applied to MRI reconstruction (1, 7–12) showing that when an image has an sparse representaton in certain domain it can be recovered from a small number of incoherent measurements.

In cardiac cine imaging intensity variations are mainly due to the movement of cardiac structures. Moving regions of the image lead to abrupt intensity changes through time that reduces the sparsity of the signal in the transformed temporal domain (13–17). As stated in (14), if the motion of elements in an image can be described with fewer parameters than the intensity changes derived from that motion, the sparsity is expected to increase by using motion modelling. In Figure 1 this approach is illustrated.

When applied to dynamic MRI reconstruction, motion estimation (ME) and motion compensation (MC) techniques lack the true dynamic image to estimate the motion information from. A common approach is to perform the ME step from an initial reconstruction of the images themselves that, however, will be affected by the artifacts introduced by the undersampling pattern that the initial reconstruction could not correct, what hinders the estimation of the true motion information. This effect becomes more relevant as the acceleration factor increases.

In k-t FOCUSS with ME/MC (15, 16) a high quality reference frame is used to perform ME by means of a block matching algorithm applied independently to each frame. The reference frame may not be available and the final reconstruction result depends heavily on its quality (17). In MASTeR (17), motion is estimated sequentially between each pair of consecutive frames. In both approaches only two frames of the sequence are available for the ME algorithm at each execution, therefore the ME algorithm cannot benefit from the additional information present in the rest of the frames making it more sensitive to artifacts in the sequence.

In this paper, and borrowing some ideas proposed in (18), the shortcomings of ME referred to above have been alleviated by adopting a groupwise (GW) approach in which the whole-sequence is registered at once to compensate for the naturally induced motion of the heart. This results in a pseudo-static sequence which, in combination with a spatio-temporal sparsifying transform, turns out to be highly sparse. We hypothesize that, given the more available information, our ME algorithm will be more robust than pairwise (PW) approaches. We call this method groupwise CS (GW-CS). Figure 1c and Supporting Video 1 illustrate the application of the GW ME/MC method. Departing from an initial reconstruction, refined reconstructed images and estimated motion information are obtained iteratively. This scheme can be easily adapted to other imaging

modalities by selecting proper ME metrics and sparsifying transforms.

Theory

CS reconstruction of undersampled dynamic MRI with ME

The CS reconstruction of undersampled MRI data is generally formulated as a constrained optimization problem given by

$$\underset{\mathbf{m}}{\text{minimize}} \|\mathbf{\Phi m}\|_{\ell 1} \quad s.t. \quad \|\mathbf{y} - \mathbf{Em}\|_{\ell 2}^2 < \epsilon \qquad [1]$$

where $\mathbf{\Phi}$ is the sparsifying transform, $\mathbf{m}$ and $\mathbf{y}$ are the dynamic MRI image to be reconstructed and the undersampled k-t data, respectively, defined as single column vectors. The encoding operator $\mathbf{E}$ performs a frame-by-frame undersampled spatial Fourier transform. In multicoil acquisitions, $\mathbf{E}$ includes the multiplication by coil sensitivities as described in (19). The threshold ϵ denotes the noise level in the acquisition. The constrained optimization problem in Eq. [1] can be converted into an unconstrained problem using a Lagrangian multiplier as follows:

$$\underset{\mathbf{m}}{\text{minimize}} \frac{1}{2} \| \mathbf{y} - \mathbf{Em} \|_{\ell_2}^2 + \lambda \| \mathbf{\Phi m} \|_{\ell_1} \qquad [2]$$

where the parameter λ establishes a trade off between data consistency and the sparsity of the solution. In CS with ME/MC, the operator $\mathbf{\Phi}$ is modified to account for the specific motion information that is present in the dynamic image at hand. In k-t FOCUSS with ME/MC (15) the unknown image $\mathbf{m}$ is decomposed into a predicted, $\mathbf{m}_{\text{pred}}$, and a residual image, $\mathbf{\Delta m}$, which is assumed to be sparse:

$$\mathbf{m} = \mathbf{m}_{\text{pred}} + \mathbf{\Delta m} \qquad [3]$$

To further increase the sparsity of the residual signal, the FT is applied along the temporal dimension of $\mathbf{\Delta m}$, denoted by the $\mathbf{F}_{\text{t}}$ operator. The optimization problem in Eq. [2] becomes

$$\underset{\mathbf{m}}{\text{minimize}} \frac{1}{2} \| \mathbf{y} - \mathbf{Em} \|_{\ell_2}^2 + \lambda \|\mathbf{F}_{\text{t}} \mathbf{\Delta m}\|_{\ell_1} \qquad [4]$$

The predicted signal $\mathbf{m}_{\text{pred}}$ is obtained by applying a block matching algorithm between each frame of $\mathbf{m}$ and a reference frame $\mathbf{m}_{\text{ref}}$. Since neither $\mathbf{m}_{\text{ref}}$ nor the true dynamic image are available for ME, a previous reconstruction step is performed with the original k-t FOCUSS algorithm without ME/MC (20).

On the other side, the MASTeR procedure does not rely on a reference frame, but motion is estimated sequentially between each pair of consecutive frames to define a set of operators that predict each frame $\mathbf{m}_i$ out of its leading and trailing frames:

$$\begin{aligned} \mathbf{m}_i &= \mathcal{F}_{i-1}\mathbf{m}_{i-1} + \mathbf{f}_i \\ \mathbf{m}_i &= \mathcal{B}_{i+1}\mathbf{m}_{i+1} + \mathbf{b}_i \end{aligned} \qquad [5]$$

where $\mathcal{F}_{i-1}$ and $\mathcal{B}_{i+1}$ denote the forward and backward MC operators. Residuals $\mathbf{f}_i$ and $\mathbf{b}_i$ are assumed to be sparse and are used as sparsity term in Eq. [2]:

$$\underset{\mathbf{m}}{\text{minimize}}\ \frac{1}{2} \parallel \mathbf{y} - \mathbf{E}\mathbf{m} \parallel_{\ell_2}^2 + \parallel \mathcal{M}\mathbf{m} \parallel_{\ell_1} \qquad [6]$$

where $\mathcal{M}\mathbf{m} = [\,\alpha\,\mathbf{f}_i^{\mathrm{T}} \,|\, \beta\,\mathbf{b}_i^{\mathrm{T}}\,]^{\mathrm{T}}$ is the weighted column-wise concatenation of both backward and forward residual terms given by Eq. [5]. For the initialization, Eq. [2] is solved using 2-D dual-tree complex-wavelet transform —DT-CWT— (21) as spatial sparsifying transform. A method also based on CWT is used for estimating inter-frame motion (22).

As explained in the introduction, ME methods described above suffer some shortcomings derived from the limited information available to the pair-wise ME algorithms. In GW-CS, we propose to jointly estimate and compensate the motion in the whole dynamic image domain. Under this approach, the optimization problem in Eq. [2] becomes

$$\underset{\mathbf{m}}{\text{minimize}}\ \frac{1}{2} \parallel \mathbf{y} - \mathbf{E}\mathbf{m} \parallel_{\ell_2}^2 + \lambda \parallel \mathbf{\Phi}\mathcal{T}_\Theta\mathbf{m} \parallel_{\ell_1} . \qquad [7]$$

where $\mathbf{\Phi}$ is a freely chosen spatio-temporal sparsifying transform and $\mathcal{T}_\Theta$ is a groupwise MC operator that will be introduced below. We should point out that in the MASTeR case the sparse representation based on the registration residuals is determined by the ME scheme itself, for which an additional transformation may not be clearly beneficial in terms of increasing sparsity. The proposed ME algorithm is detailed in the next section.

Temporal groupwise registration for ME/MC

To introduce the registration method it is convenient to redefine the dynamic MRI sequence $\mathbf{m}$ as a set of spatially continuous images $m = \{m_1(\mathbf{x}), m_2(\mathbf{x}), \ldots, m_N(\mathbf{x})\}$, with $1 \leq n \leq N$ a temporal index and $m_n(\mathbf{x})$ defined over the space $\mathbf{x} \in \mathcal{X} \subset \mathbb{E}^2$. The registration procedure consists in finding a set of spatial transformations $T = \{T_n : \mathbf{x}'_n = T_n(\mathbf{x})) \in \mathcal{X}\}$ such that the cost function given by

$$H(T; m) = \int_{\mathcal{X}} V(m_1(T_1(\mathbf{x})), \ldots, m_N(T_N(\mathbf{x})))\mathrm{d}\mathbf{x} \qquad [8]$$

is minimized (18). The solution is constrained to those sets of transformations with the average deformation of each position equal to the identity transformation (23):

$$\frac{1}{N}\sum_{n=1}^{N} T_n(\mathbf{x}) = \mathbf{x} \qquad [9]$$

In Eq. [8], the integrand $V(m_1(T_1(\mathbf{x})), \ldots, m_N(T_N(\mathbf{x}))) = V(\mathbf{x})$ is the similarity metric used to measure the point by point similarity between the set of images. In cardiac cine MRI, the intensity change of the image along time is mainly due to the movement of the heart, so a least squares metric based on the variance of the intensity (VI) along time may suffice (24):

$$V(\mathbf{x}) = \frac{1}{N}\sum_{n=1}^{N}\left(m_n(T_n(\mathbf{x})) - \frac{1}{N}\sum_{k=1}^{N} m_k(T_k(\mathbf{x}))\right)^2. \qquad [10]$$

There is also a need for an adequate deformation model. The proposed algorithm employs a 2D free form deformation (FFD) model based on B-splines (25), which has been widely used in practice. The FFDs are based on a parametric model that deforms an object by manipulating an underlying mesh of M control points $\Theta = \{\theta_{k,n}\}$, with $1 \le k \le M, 1 \le n \le N$, uniformly spaced in $\mathcal{X}$. Then the set of deformations T is parametrized by Θ, a fact that we denote by $T = T_\Theta$.

To constrain the estimated deformation to be smooth, in concordance with the expected deformation of anatomical structures (25), a penalty regularization term is introduced in Eq. [8] given by:

$$C(T_\Theta) = \frac{1}{|\mathcal{X}|N}\sum_{n=1}^{N}\int_{\mathcal{X}} \alpha\left(\left|\frac{\partial^2 T_n(\mathbf{x})}{\partial x^2}\right|^2 + \left|\frac{\partial^2 T_n(\mathbf{x})}{\partial y^2}\right|^2 + 2\left|\frac{\partial^2 T_n(\mathbf{x})}{\partial x \partial y}\right|^2\right) + \beta\left|\frac{\partial^2 T_n(\mathbf{x})}{\partial n^2}\right|^2 \mathrm{d}\mathbf{x} \qquad [11]$$

where $(x, y)^{\mathrm{T}} = \mathbf{x}$. We add a temporal regularization term in order to favor smoothness in the temporal trajectory based on temporal derivatives approximated by finite differences. Given the quasi-periodic motion of the heart the last frame in the sequence is considered to be followed by the first one. α and β parameters used to weight the spatial and temporal regularization terms, respectively. The resulting regularized non-rigid GW registration is then formulated as

$$\underset{\Theta}{\text{minimize}}\ H(T_\Theta; m) + C(T_\Theta) \qquad [12]$$

and the groupwise MC operator $\mathcal{T}_\Theta$ in Eq. [7] is defined as the discretized version of T_Θ.

Reconstruction algorithm

Since at the very beginning of the algorithm we do not have any data from which motion information can be estimated, we have resorted to the common approach (14, 15, 17) of making use of a regular

CS reconstruction prior step; then an iterative procedure consisting in a ME/MC step followed by a MC-CS reconstruction step, is adopted. In our implementation a predefined number of iterations has been set; it is very simple to use some alternative convergence criterion instead. A pseudocode description of the algorithm follows:

Groupwise registration based CS reconstruction of Undersampled Dynamic MRI.

---

input:

$\mathbf{y}$: undersampled k-t data

$\mathbf{E}$: encoding operator

$\mathbf{\Phi}$: sparsifying transform

$\lambda, \lambda_{s/t}$: sparsity regularization parameters

α, β: ME/MC regularization parameters

initialization:

$k \leftarrow 0$

% Solve regular CS reconstruction problem in Eq. [2]:

$\mathbf{m}_0 \leftarrow \arg\min_{\mathbf{m}} \|\mathbf{y} - \mathbf{E}\mathbf{m}\|_{\ell_2}^2 + \lambda \|\mathbf{\Phi}\mathbf{m}\|_{\ell_1}$

while $k <$ max. number of iterations **do**

% Temporal registration: Solve Eq. [12]

$\Theta_{k+1} \leftarrow \arg\min_{\Theta} H(T_\Theta; \mathbf{m}_k) + C(T_\Theta)$

% MC-CS reconstruction: Solve Eq. [15] (as opposed to [7], see Implementation section) with estimated motion parameters.

$$\underset{\mathbf{m}}{\text{minimize}} \; \frac{1}{2} \parallel \mathbf{y} - \mathbf{E}\mathbf{m} \parallel_{\ell_2}^2 + \lambda \parallel \left[\; (\mathbf{\Phi}_{\mathrm{t}} \mathcal{T}_\Theta)^{\mathrm{T}} \mid \lambda_{\mathrm{s/t}} \mathbf{\Phi}_{\mathrm{s}}^{\mathrm{T}} \; \right]^{\mathrm{T}} \mathbf{m} \parallel_{\ell_1} .$$

$k \leftarrow k + 1$

end

output: $\mathbf{m}_k$

Methods

In this section the procedures followed to implement and to validate the proposed algorithm are described. First, our hypothesis on the superiority of the GW approach *vs.* the PW counterpart is tested. Details of the method implementation and parameter selection are also provided. The

quality of the reconstructions have been tested both with quantitative metrics and the subjective judgment of expert clinicians.

Groupwise and pairwise registration comparison

In order to validate the hypothesis that the proposed GW registration algorithm performs better than an equivalent PW approach, the following experiment was carried out:

1. A SSD registration metric equivalent to the PW version of the metric in Eq. [10] was defined as

$$V(\mathbf{x}) = \frac{1}{N}\sum_{n=1}^{N}\left(m_n(T_n(\mathbf{x})) - m_{ref}(\mathbf{x})\right)^2. \qquad [13]$$

   where m_{ref} denotes the frame selected as a reference. We choose a diastolic frame, where lower cardiac motion is present.

2. The ME algorithm was applied to an initial regular CS reconstruction of a sequence from a healthy volunteer, for undersampling factors of the k-space data (r) ranging from one (no undersampling) to 16. The deformation fields obtained for the GW and PW metrics are denoted as $T^r_{GW}(\mathbf{x})$ and $T^r_{PW}(\mathbf{x})$, respectively. We define the registration error (RE) committed due to the presence of undersampling artifacts as —for the GW metric—:

$$RE_{GW}(r) = \int_{\mathcal{X}} \|T^1_{GW}(\mathbf{x}) - T^r_{GW}(\mathbf{x})\|^2 \mathrm{d}\mathbf{x}. \qquad [14]$$

   The definition for the PW method is analogous. The behavior of $RE(r)$ denotes how fast the registration degrades due to the increasing presence of undersampling artifacts.

Algorithm implementation

The GW-CS reconstruction was performed in MATLAB (MathWorks, Natick, MA). The optimization problems in Eqs. [2] and [7] related to the reconstruction steps have been solved using the NESTA algorithm (26). For the initialization of the algorithm, spatial DT-CWT of each frame was used as sparsifying transform $\mathbf{\Phi}$, in order to get the same initial reconstruction than MASTeR. A nonlinear conjugate gradient algorithm with backtracking line search (27) has been used to solve the registration problem in Eq. [12]. Additional fixed control points were placed outside the image domain in order to guarantee that the spatial transformation is properly defined inside the domain.

In the following reconstruction steps, the sparsifying transform $\mathbf{\Phi}$ in Eq. [7] may comprise both spatial and temporal dimensions transforms. However, we should make some considerations: given

the discrete nature of the reconstructed images, the application of the MC operator involves an interpolation step that implies unavoidable errors. As we could verify, the interpolation process may distort the reconstruction result, as illustrated in Figure 2. Since the MC operator introduces a spatial low pass filtering as a side effect, high spatial frequency components in the reconstructed image are not present in the image used in the ℓ_1 regularization term in Eq. [7]. Furthermore, since only only a small fraction of the high frequency coefficients is acquired, data mismatch in high frequency components is not properly penalized by the data fidelity term.

To overcome this limitation, we split the spatio-temporal sparsifying transform in Eq. [7] into a temporal transform applied to the motion compensated sequence and a spatial transform applied to the original sequence without MC. That is, we actually solve the optimization problem given by

$$\underset{\mathbf{m}}{\text{minimize}}\ \frac{1}{2}\parallel \mathbf{y}-\mathbf{E}\mathbf{m}\parallel_{\ell_2}^2+\lambda\parallel\left[\ (\mathbf{\Phi}_{\mathrm{t}}\mathcal{T}_{\Theta})^{\mathrm{T}}\mid\lambda_{\mathrm{s/t}}\mathbf{\Phi}_{\mathrm{s}}^{\mathrm{T}}\ \right]^{\mathrm{T}}\mathbf{m}\parallel_{\ell_1}. \qquad [15]$$

where $\lambda_{\mathrm{s/t}}$ weights the spatial sparsity vs. temporal sparsity.

Undersampled data was also reconstructed using k-t FOCUSS with ME/MC and MASTeR. To this end, the code available at at http://users.ece.gatech.edu/∼sasif/dynamicMRI from the authors of (17) with minor adaptations was used. For the k-t FOCUSS reconstruction, a set of diastole cardiac phase frames from each dataset was manually selected and its temporal average used as a reference frame to obtain the predicted signal $\mathbf{m}_{\mathrm{pred}}$ in Eq. [3]. The number of ME-reconstruction iterations of MASTeR and GW-CS was set to four.

Data acquisition

Three different datasets have been employed, two with healthy volunteers and one with patients diagnosed with hypertrophic cardiomyopathy (HCM). In all the cases a regular, fully sampled, multislice 2D BH cardiac cine MRI study was acquired. The fully sampled data was retrospectively undersampled using a Gaussian variable-density random undersampling pattern along the phase encoding direction. Eight central lines of the k-space were always selected and sensitivity maps were obtained from separate scans. All the scans were performed in accordance with the Research Ethics Board of our institutions and each subject provided informed consent. Each of the datasets are described at continuation.

Multi-Coil data of healthy volunteers

One healthy volunteer was scanned on a 1.5T Philips scanner (Philips Healthcare, The Nether-

lands) with a 32-element cardiac coil employing a b-SSFP sequence. Relevant scan parameters include: TR/TE/flip angle = 2.8ms/1.39ms/60°, FOV = 320 × 320mm^2, spatial resolution = 2 × 2 mm^2, slice thickness = 8mm with no gap between slices. 16 cardiac phases were reconstructed.

A short axis MRI scan made available by the authors of (17) was also used for reconstruction of multi-coil data. The dataset was acquired using a General Electric 1.5T TwinSpeed scanner with a 5-element cardiac coil and a FIESTA/FastCARD cine steady-state free precession sequence, with following parameters: TE/TR/flip angle = 2.0ms/4.1ms/45°, FOV = 350 × 350 mm^2, 224 × 256 matrix reconstruction and 16 temporal frames.

Single-Coil data of healthy volunteers and HCM patients

Three healthy volunteers were scanned on a 3T Philips scanner with a 32-element cardiac coil. Other relevant scan parameters include: b-SSFP sequence, TR/TE/flip angle = 3.3ms/1.57ms/45°, FOV = 320×320mm^2, 30 cardiac phases, and slice thickness = 8 mm. Three patients diagnosed with HCM were scanned with a 16-element antenna and the same parameters, excluding: TR/TE/flip angle = 6ms/3ms/25° and FOV = 425 × 425 mm^2. Since no raw data were available, reconstructed DICOM sequences were converted back into k-t space and considered as single coil acquisitions.

Quantitative metrics comparison

Two quantitative error metrics were used for comparison of the reconstructions. Firstly, the signal-to-error ratio (SER), defined as

$$\mathrm{SER(dB)} = 20 \log_{10} \frac{\|\mathbf{m}\|_{\ell_2}}{\|\mathbf{m} - \hat{\mathbf{m}}\|_{\ell_2}},$$

where $\mathbf{m}$ denotes the fully sampled image and $\hat{\mathbf{m}}$ the image reconstructed from the undersampled data. Second, the structural similarity index —SSIM— (28) was also used as a quantitative metric that better represents image quality.

Subjective image quality review from clinicians

For a set of three healthy volunteers and three patients affected by HCM the reconstructions obtained with k-t FOCUSS, MASTeR and the proposed method for acceleration factors 4, 6 and 8 were blindly reviewed and rated by three experts[1]. For each dataset and acceleration factor, the reconstructions obtained with each method were simultaneously presented on the screen sorted

[1]Namely, the two cardiologists Dr. A. Revilla, and Dr. T. Sevilla and the radiologist Dr. J. Calabia, all of them from the Hospital Clínico Universitario of Valladolid, Spain

randomly to the experts, who were asked to rate them attending to their general quality. The results were collected via a web form. Each expert rated two controls and two cases, so each individual has been rated by two experts.

Parameter selection

To select those registration parameters α and β that make the registration algorithm most robust against the undersampling artifacts without compromising the estimation of the true cardiac motion, the ME algorithm was applied to an initial CS reconstruction of a healthy volunteer sequence undersampled by a factor of 6. α and β were chosen to minimize the residual motion —measured as the temporal TV of the resulting sequence— when the motion fields thus obtained were applied to the original, fully sampled image. The optimal values of α and β did not show significant variation for other acceleration factors considered. Moreover, the final reconstruction results have shown to be robust to the choice of α and β in a wide range of values for all the datasets used since the heart dimensions and the field of views do not differ considerably in all the datasets used.

The reconstruction parameters λ and $\lambda_{s/t}$ and their equivalent counterparts in the compared methods (see (20) and (17)) were fitted to get the highest SER in the reconstruction of the 1.5T (5 coils) dataset, one of the 3T datasets (DICOM data) and the 32-coil dataset. An example of the sensitivity of both SER and SSIM (see Results section) is shown in the Supporting Figure 1 for the latter dataset. Notice that the axis are in logarithmic scale. These parameters have been used for the experiments described below with the only exception of the subjective judgment on the three HCM patients; in that experiment, since the acquisition signal to noise ratio was considerably smaller —a different cardiac antenna was used—, the SER did not turn out to be a satisfactory metric; on these data, the parameters for the subjective judgment experiment have been set, for the three methods, by maximizing the visual judgment of a different observer than the experts on a single patient.

Final reconstructions were obtained for an acceleration factor of 4 with three different sparse transforms applied in the initialization of the algorithm, namely, temporal FFT, temporal TV and spatial DT-CWT. Results are fairly similar for the three reconstruction procedures since no structural differences are appraised; some subtle high frequency artifacts are present with TV and DT-CWT, but all of them fall outside the cardiac area. Since we mean to compare our algorithm with MASTeR, we have chosen DT-CWT for initialization.

Results

Groupwise and pairwise methods comparison

Figure 3 shows on top the RE values defined for the GW case in Equation 14 for different values of the acceleration factor. We also show the corresponding RE values for the PW case. The figure on the bottom shows the total variation of the residual image obtained after registration. Both cases (GW and PW) are shown.

Figure 4 illustrates the effect of a corrupted ME in a MASTeR reconstruction of a retrospectively 10-fold undersampled short axis cardiac cine sequence. As remarked in Figure 4b, in the final reconstruction false motion is introduced in the original sequence. In Figure 4c temporal evolution of a single pixel is plotted. The reconstructed pixel intensity fluctuates along time, an effect that is perceived by a human observer as a spatial vibration when observing the dynamic sequence. The temporal TV values in Figure 4d illustrates the false motion introduced (in Supporting Video 2 the effect is clearly appreciable). For comparison, in the sequence reconstructed with GW-CS with spatial TV sparsification the effect is not present.

Figure 5 and Supporting Video 3 show the reconstruction results of k-t FOCUSS, MASTeR, and the proposed GW-CS with two spatial sparsifying transforms, TV and CWT, at a high acceleration factor of 12, for the 1.5T dataset. Supporting Video 4 shows the same results for one of the acquired 3T short axis datasets. Results indicate that GW-CS with TV or CWT provides lower error than the rest of the methods. The temporal evolution of a slice is also represented. In Figure 6 the proposed algorithm is applied to the dataset from a patient with abnormal cardiac motion. A similar performance of the algorithm can be observed as the temporal behaviour of the cardiac structures is preserved; this is illustrated in the last row of the figure for a vertical line taken at the center of the image, and can be more clearly appreciated in the Supporting Video 5.

Quantitative metrics results

In order to evaluate the performance of the different methods along the cardiac cycle, Figure 7 shows quantitative quality measures calculated for each reconstructed frame of the same dataset as before in terms of the SER and the SSIM introduced in the previous section, where the fully sampled image is used as reference. In Figure 8 the performance of the compared methods for different acceleration factors is analyzed. SER and SSIM index are calculated over a ROI around the heart and plotted vs. the acceleration factor. Figure 9 shows the reconstruction of a SA slice

from the 32-multicoil 1.5T equipment in the different time instants of the cardiac cycle; the figure also shows plots of the resulting SER and SSIM. In the Supporting Video 6, results for acceleration factors of 1, 2, 4, 8, 12 are available.

Subjective qualification results

The reviews reported by the clinicians are summarized in table 1. The values in the table indicate the number of times the reconstruction obtained with each method was selected as the best one for each acceleration factor.

Discussion

As illustrated in Figures 4 and 5, GW-CS gets better results than k-t FOCUSS or MASTeR. Less noisy images and smoother interior cavities are recovered while preserving sharp edges at the myocardium wall and small structures. GW-CS with CWT spatial sparsification preserves fine texture details in the image better than TV. Most significant differences can be appreciated in the temporal evolution of a single slice for each reconstruction. With k-t FOCUSS, fine motion details are lost, as can be observed in the interior wall of the myocardium at mid-diastole phase, indicated by arrows in the figure. With MASTeR, the temporal evolution gets noticeably corrupted by an erratic motion that can be most clearly observed in the right ventricle wall. The erratic motion becomes evident when observing the dynamic reconstructions as a video sequence (see Supporting Video 2). A key aspect of cardiac cine MRI for clinical application is the information it provides about myocardium dynamics, so images corrupted by erratic motion may be an issue. This statement seems to be further supported by the subjective judgements of the experts shown in Table 1. When applied to cases of abnormal cardiac motion —an HCM patient— the algorithm has shown to perform in a similar way than in the healthy volunteers case (see Figure 6).

From the quantitative evaluation plotted in Figure 7, we can determine that GW-CS obtains better scores than k-t FOCUSS or MASTeR along the vast majority of cycles in the cardiac cycle, both in phases with faster motion of the heart (systole) as well as in slower phases. SER differences in the ROI are within the range of 1–2 dB. During the diastole phase, k-t FOCUS results get close to MASTeR and GW-CS. These are the frames used as reference for the k-t FOCUSS ME step, with small heart motion. Results over the whole image show wider differences, of about 3dB, between GW-CS with CWT and MASTeR. In this case, the difference may be due to the erratic

motion introduced by the MASTeR ME method. Results over the whole image also indicate that GW-CS with CWT spatial transform gets better results than spatial TV in the static areas outside the ROI.

Results obtained by GW-CS with CWT or TV for the reconstruction of the 1.5T dataset, illustrated in Figure 8, are very close to those obtained by MASTeR. Indeed, for low acceleration factors our method gets slightly worse quantitative metrics than MASTeR. However, in the 3T data experiments, GW-CS outperforms the others for acceleration factors equal or higher than 6. The difference in the results can be explained by two aspects: firstly, the fully sampled 1.5T dataset has an appreciable noise level; during the CS reconstructions part of the noise is washed out by our spatio-temporal sparsity terms. In these situation, the noise removal effect degrades the calculated SER value. 3T data have higher apparent SNR, so this effect is not so relevant. Secondly, the 1.5T data consists of 16 reconstructed cardiac phases, vs. the 30 available in the 3T data. Therefore, much more information is available to the GW-ME method than in the 1.5T dataset. The MASTeR ME method cannot take advantage of the more information available since motion is only estimated between pairs of adjacent frames. Finally, for 32 coil data (recall Figure 9) if the plots in this figure are compared with those in Figure 8 one can appraise a similar behavior. Therefore, conclusions from 32-elements seem parallel to those previously described.

All in all, in these reconstructions still some high frequency artifacts are appraised, which constitutes a current limitation of our method. Nevertheless, the reviews reported by the clinicians (Table 1) indicate that the proposed method outperforms the other other two in terms of subjective perception as well; these differences, in addition, seem to have an increasing trend with the acceleration factor in accordance with the quantitative results obtained in the previous comparison.

In the experimental section we have pursued to compare the performance of the different ME/MC procedures; consequently, all experimental conditions have remained the same, i.e., same undersampling patterns, initialization reconstructions, optimization method and sparsifying transforms have been used. Therefore, we understand that the main source of improvement in our results are due to the superior ME/MC scheme. The B-spline deformation model used is able to accurately describe the motion of the heart and enables us to easily introduce the regularization term in Eq. [11] that makes it more robust against artifacts in the image. As can be seen in the results section, the quantitative differences between MASTeR and GW-CS increase with the reduction factor. This indicates that the GW approach is able to maintain accurate motion estimation even from highly undersampled data. This statement is supported by means of Figure 3; the figure shows that both

in terms of RE and in terms of TV of the residual image after registration, the GW approach shows a better performance than the PW counterpart and the parameter RE seems to highlight differences between the two paradigms as the acceleration factor increases.

We would like to point out the effect of ME errors in the reconstructed signal. Fine motion details that the motion model was not able to incorporate were lost in the reconstructed signal. Therefore, to have a robust and versatile motion model is a key aspect in ME/MC based reconstruction methods; Figure 6 shows that our method is able to track abnormal motion as well.

In our experiments, the reconstruction parameters used with the volunteers data were set using only one of the three 3T available acquisitions. However, as previously stated, due to the lower SNR in the patients acquisitions these parameters had to be modified. This indicates, as the compressed sensing theory establishes (5, 6), that λ and $\lambda_{s/t}$ optimal values strongly depend on the SNR of the acquisitions. This is a common limitation in several CS based reconstruction algorithms that should be addressed. In any case, the parameters were set using only one patient, and they carried over satisfactorily to the other two. On the contrary, the registration parameters α and β have been fitted only once for all the experiments. Although their optimal values could change for image modalities with very different contrast or spatio-temporal resolution, these circumstances can be known beforehand. This suggest that in real practice a calibration procedure can be designed.

The GW registration method proposed is more computationally demanding than their PW counterparts, since an optimization problem of higher dimensionality is addressed. However, in our experiments, the computational cost associated to the registration procedure is much lower than the cost of the reconstruction step. Therefore, the relative increase in computational cost due to the registration step has not a considerable effect in the overall algorithm cost.

Conclusions

In this paper we have presented a new CS reconstruction algorithm (GW-CS) based on a regularized, temporal, groupwise registration method. In the proposed algorithm, the whole sequence information is available to the ME method at each registration step instead of just a reference and current frame —as in k-t FOCUSS— or pairs of adjacent frames —as in MASTeR—. This makes the registration method robust to the incoherent aliasing that appears in highly undersampled data enabling robust estimation of the motion information in the dynamic sequence and achieving further acceleration factors for the same image quality after reconstruction. The non-rigid nature of

the B-spline deformation model employed has shown capable of describing the motion of the heart and to recover finer motion details than the block matching method used in k-t FOCUSS.

We understand that our ME/MC scheme is quite flexible: first, the ME method can be easily extended to other image modalities by proper election of the similarity metric. Second, the quasi-static sequence obtained after MC can be highly sparsified by any appropriate transform which may depend on the image modality. Third, the scheme seems compatible with other acquisition strategies rather than Cartesian trajectories (9). Finally, given the high acceleration factors achieved, the proposed approach could be naturally extended to real-time imaging of the heart or other moving parts of the body (29). These possibilities will be explored in future work.

Acknowledgments

The authors would like to thank Claudia Prieto and Muhammad Usman collaboration in the acquisition of the 1.5T raw data at King's College London. This work was partially supported by the Junta de Castilla y León under grant VA136U13, Instituto de Salud Carlos III PI11-01492, Ministerio de Economía y Competitividad under grant TEC2013-44194-P and by the University of Valladolid and Banco Santander FPI-UVa Fellowship Program.

References

1. Feng L, Srichai MB, Lim RP, Harrison A, King W, Adluru G, Dibella EV, Sodickson DK, Otazo R, Kim D. Highly accelerated real-time cardiac cine MRI using k–t SPARSE-SENSE. Magn Reson Med 2013;70:64–74.

2. Chandarana H, Block TK, Rosenkrantz AB, Lim RP, Kim D, Mossa DJ, Babb JS, Kiefer B, Lee VS. Free-breathing radial 3d fat-suppressed t1-weighted gradient echo sequence: a viable alternative for contrast-enhanced liver imaging in patients unable to suspend respiration. Investigative Radiology 2011;46:648–653.

3. Tsao J, Boesiger P, Pruessmann KP. k-t BLAST and k-t SENSE: Dynamic MRI with high frame rate exploiting spatiotemporal correlations. Magn Reson Med 2003;50:1031–1042.

4. Huang F, Akao J, Vijayakumar S, Duensing GR, Limkeman M. k-t GRAPPA: A k-space implementation for dynamic MRI with high reduction factor. Magn Reson Med 2005;54:1172–1184.

5. Candès E, Romberg J, Tao T. Robust uncertainty principles: exact signal reconstruction from highly incomplete frequency information. IEEE Trans Inf Theory 2006;52:489–509.

6. Donoho D. Compressed sensing. IEEE Trans Inf Theory 2006;52:1289–1306.

7. Lustig M, Donoho D, Pauly JM. Sparse MRI: The application of compressed sensing for rapid MR imaging. Magn Reson Med 2007;58:1182–1195.

8. Otazo R, Kim D, Axel L, Sodickson DK. Combination of compressed sensing and parallel imaging for highly accelerated first-pass cardiac perfusion MRI. Magn Reson Med 2010;64:767–776.

9. Usman M, Atkinson D, Odille F, Kolbitsch C, Vaillant G, Schaeffter T, Batchelor PG, Prieto C. Motion corrected compressed sensing for free-breathing dynamic cardiac mri. Magn Reson Med 2013;70:504–516.

10. Chen X, Salerno M, Yang Y, Epstein FH. Motion-compensated compressed sensing for dynamic contrast-enhanced MRI using regional spatiotemporal sparsity and region tracking: block low-rank sparsity with motion-guidance (BLOSM). Magn Reson Med 2014;72:1028–1038.

11. Lingala S, DiBella E, Jacob M. Deformation corrected compressed sensing (DC-CS): A novel framework for accelerated dynamic MRI. IEEE Trans Med Imag 2015;34:72–85.

12. Yoon H, Kim KS, Kim D, Bresler Y, Ye JC. Motion adaptive patch-based low-rank approach for compressed sensing cardiac cine MRI. IEEE Trans Med Imag 2014;33:2069–2085.

13. Irarrazaval P, Boubertakh R, Razavi R, Hill D. Dynamic three-dimensional undersampled data reconstruction employing temporal registration. Magn Reson Med 2005;54:1207–1215.

14. Prieto C, Batchelor PG, Hill D, Hajnal JV, Guarini M, Irarrazaval P. Reconstruction of undersampled dynamic images by modeling the motion of object elements. Magn Reson Med 2007;57:939–949.

15. Jung H, Sung K, Nayak KS, Kim EY, Ye JC. k-t FOCUSS: A general compressed sensing framework for high resolution dynamic MRI. Magn Reson Med 2009;61:103–116.

16. Jung H, Ye JC. Motion estimated and compensated compressed sensing dynamic magnetic resonance imaging: What we can learn from video compression techniques. Int J Imag Syst Tech 2010;20:81–98.

17. Asif MS, Hamilton L, Brummer M, Romberg J. Motion-adaptive spatio-temporal regularization for accelerated dynamic MRI. Magn Reson Med 2013;70:800–812.

18. Cordero-Grande L, Merino-Caviedes S, Aja-Fernández S, Alberola-López C. Groupwise elastic registration by a new sparsity-promoting metric: Application to the alignment of cardiac magnetic resonance perfusion images. IEEE Trans Pattern Anal 2013;35:2638–2650.

19. Pruessmann KP, Weiger M, Scheidegger MB, Boesiger P. SENSE: Sensitivity encoding for fast MRI. Magn Reson Med 1999;42:952–962.

20. Jung H, Ye JC, Kim EY. Improved k–t BLAST and k–t SENSE using FOCUSS. Phys Med Biol 2007;52:3201.

21. Selesnick I, Baraniuk R, Kingsbury N. The dual-tree complex wavelet transform. IEEE Signal Process Mag 2005;22:123–151.

22. Magarey J, Kingsbury N. Motion estimation using a complex-valued wavelet transform. IEEE Trans Signal Process 1998;46:1069–1084.

23. Bhatia KK, Hajnal JV, Puri BK, Edwards AD, Rueckert D. Consistent groupwise non-rigid registration for atlas construction. In Proceedings of IEEE ISBI. Arlington, VA, USA 2004; pp. 908–911.

24. Metz C, Klein S, Schaap M, van Walsum T, Niessen W. Nonrigid registration of dynamic medical imaging data using nD + t B-splines and a groupwise optimization approach. Med Image Anal 2011;15:238–249.

25. Rueckert D, Sonoda LI, Hayes C, Hill DLG, Leach MO, Hawkes D. Nonrigid registration using free-form deformations: application to breast MR images. IEEE Trans Med Imag 1999; 18:712–721.

26. Becker S, Bobin J, Candès E. Nesta: A fast and accurate first-order method for sparse recovery. SIAM Journal on Imaging Sciences 2011;4:1–39.

27. Nocedal J, Wright S. Numerical Optimization. New York: Springer 1999. 664 p.

28. Wang Z, Bovik A, Sheikh H, Simoncelli E. Image quality assessment: from error visibility to structural similarity. IEEE Trans Image Process 2004;13:600–612.

29. Uecker M, Zhang S, Voit D, Merboldt KD, Frahm J. Real-time MRI: recent advances using radial FLASH. Imaging Med 2012;4:461–476.

Figures captions

Figure 1: (a) Selected frames from cine MRI sequence with estimated material point trajectory along time (continuous line) vs. fixed spatial position (dashed line). (b) Pixel intensity variation along time and along estimated motion trajectory. (c) Temporal evolution of a single slice in original sequence (left) and after compensate the estimated motion. Temporal TV (d) and temporal log-FT (e) of the original and motion compensated sequences. In (d), a noticeable reduction in the TV values can be observed. In (e), the Fourier coefficients get more concentrated around the DC and low frequency components, i.e., the MC procedure contributes to obtain a sparser representation in the x-f space.

Figure 2: Effect of the interpolation in the reconstructed signals. (a) from left to right: detail of the original sequence to be reconstructed with estimated motion deformation superposed for better visualization, same region after MC, motion compensated reconstructed sequence and final reconstructed sequence with spatial sparsity constrain applied to the motion compensated sequence. In the last case, the high frequency artifact present in the reconstructed signal has been removed by the deformation/interpolation operator. (b) from left to right: original fully sampled k-space data, undersampled data, k-space data of the reconstructed sequence after MC and k-space data of the final reconstructed sequence.

Figure 3: (top) Residual temporal Total Variation of the image after registration and (bottom) Registration Error (see Eq. 14) both for GW and PW approaches as a function of the acceleration factor.

Figure 4: Effect of the corrupted ME on a short axis 10-fold undersampled cardiac cine sequence. (a) First frame of the original sequence. (b) Temporal evolution of the intensity profile at the location indicated in (a) by the dashed line. (c) Plot of intensity value along time of the pixel indicated by the arrow in (b), from the fully sampled and reconstructed sequences. (d) Temporal TV of original and final reconstructions.

Figure 5: Short axis CINE reconstructions with the fully sampled data and k-t FOCUSS, MASTeR and the proposed GW-CS with TV and CWT as spatial sparsifying transforms with retrospective 12-fold undersampling. Single frame (top) and temporal evolution at the location indicated by dashed line (bottom). Middle row shows the absolute error of each image. Arrows in the bottom row indicate regions where fine motion detail has been lost in k-t FOCUSS.

Figure 6: Reconstructions of the data from a patient with a diagnosed HCM for different values of the subsampling factor. As it can be observed, the most relevant information, is preserved in the final sequence. The last row in the figure represents the intensity profile of a vertical line taken at the center of the image. The intensity variation highlights that motion is preserved.

Figure 7: Quantitative quality measures for each frame on a 12-fold accelerated reconstruction of each dataset used. SER and SSIM index calculated over a ROI containing the heart and over the whole image. First column corresponds to the 1.5T data ad the remaining three columns to the 3T data.

Figure 8: SER and SSIM index calculated over a ROI around the heart for the four reconstructed sequences. First columnn corresponds to 1.5T data and the remaining three columns to the 3T data.

Figure 9: (left) Reconstruction of 32-coil acquisitions for different values of the acceleration factor; three instants of the cardiac cycle are shown from top to bottom; (right) SER and SSIM (in the whole image —blue— and within a ROI around the myocardium —green— as function of the acceleration factor for the images shown.

Supporting material

Supporting Figure 1: Reconstruction parameters selection. One of the multicoil datasets has been reconstructed for a fixed acceleration factor of 6 with several possible values of the parameters λ_t and $\lambda_{s/t}$. The final parameters are chosen so that the quality metrics SER and SSIM get maximun values. The optimal values of the parameters could vary for different signals and acceleration factors; however, no significant differences have been observed. Therefore, λ_t and $\lambda_{s/t}$ remained the same in the rest of the experiments.

Video 1: Video showing the effect of the groupwise motion compensation operator. The fully sampled 1.5T sequence is played on the left half of the video and the motion compensated one on the right half. The whole sequence is displayed followed by a zoom of a ROI around the heart. The estimated spatial deformation is superposed for visualization.

Video 2: Video showing the effect of corrupted motion estimation on the final reconstruction. A fully sampled acquired 3T sequence is played on the left part. In the center and right parts a MASTeR and a GW-CS with TV reconstructions of the 10-fold undersampled sequence is shown. MASTeR reconstruction presents a motion artifact due to error induced by non-coherent aliasing during motion estimation.

Video 3: Video showing the reconstructions of the 1.5T dataset with a 12-fold acceleration factor. From left to right: fully sampled sequence, k-t FOCUSS with ME/MC, MASTeR, GW-CS with TV and GW-CS with CWT are shown.

Video 4: Video showing the reconstructions of one of the 3T acquired datasets with a 12-fold acceleration factor. From left to right: fully sampled sequence, k-t FOCUSS with ME/MC, MASTeR, GW-CS with TV and GW-CS with CWT are shown.

Video 5: Video showing the reconstructions of a sequence with abnormal cardiac motion. From left to right: fully sampled sequence and acceleration factors of 2, 4 and 8.

Video 6: Video showing the reconstructions of a 32-coil, healthy volunteer dataset. From left to right, fully sampled sequence and acceleration factors of 2, 4, 8 and 12. In the last two cases, high frequency artifacts and loss of quality become relevant.

Table 1: Clinial experts qualification results. The values indicate the number of times that each reconstruction was in first place in the reported qualifications

	Accel. factor	GW-CS	MASTeR	k-t FOCUSS
Healthy volunteers	4	4	1	1
	6	5	0	1
	8	6	0	0
HCM patients	4	4	1	1
	6	5	0	1
	8	4	0	2

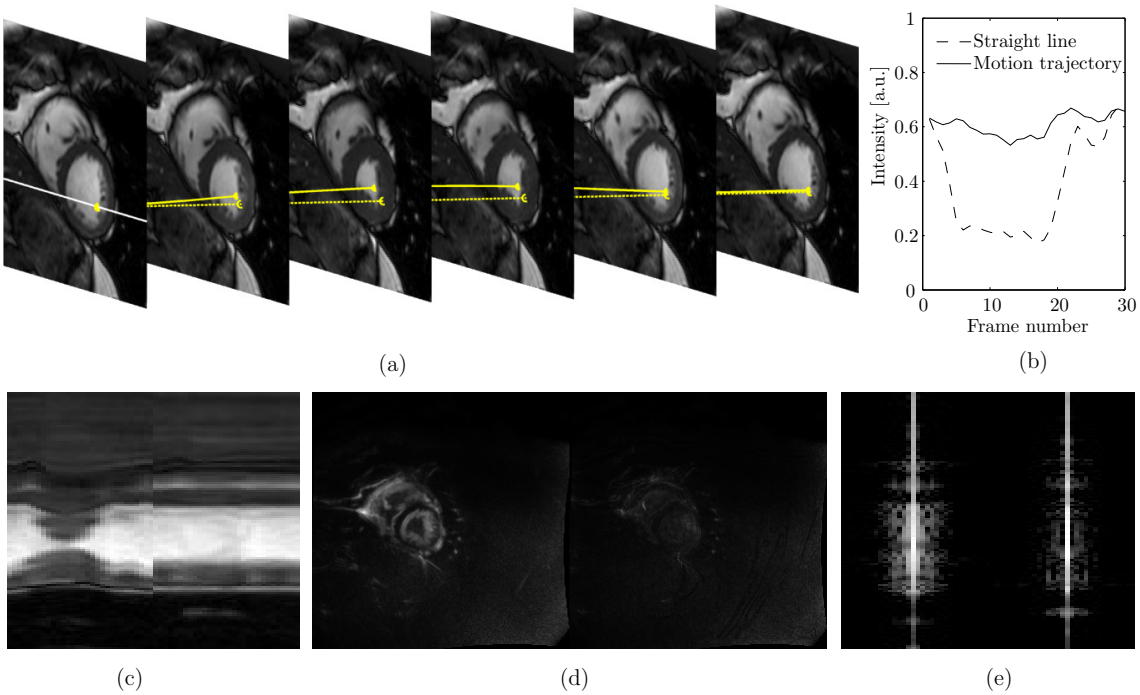

Figure 1: (a) Selected frames from cine MRI sequence with estimated material point trajectory along time (continuous line) vs. fixed spatial position (dashed line). (b) Pixel intensity variation along time and along estimated motion trajectory. Lower and smoother intensity transitions are present in the second case. (c) Temporal evolution of a single slice in original sequence (left) and after compensate the estimated motion. Temporal TV (d) and temporal log-FT (e) of the original and motion compensated sequences. In (d), a noticeable reduction in the TV values can be observed. In (e), the Fourier coefficients get more concentrated around the DC and low frequency components, i.e., the MC procedure contributes to obtain a sparser representation in the x-f space.

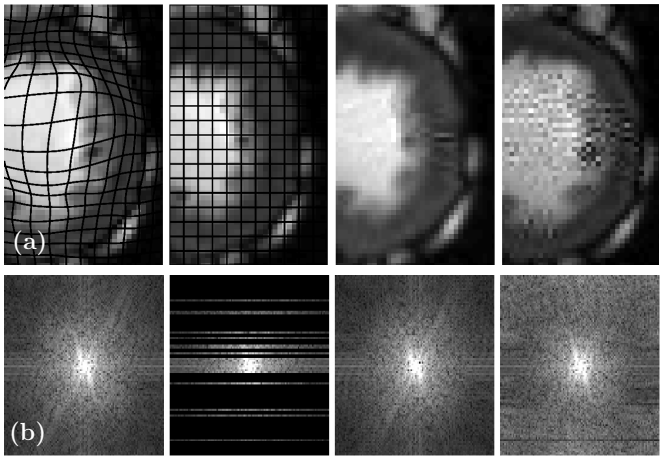

Figure 2: Effect of the interpolation in the reconstructed signals. (a) from left to right: detail of the original sequence to be reconstructed with estimated motion deformation superposed for better visualization, same region after MC, reconstructed sequence with spatial sparsity constrain applied to the motion compensated sequence and reconstructed image after MC. In the last case, the high frequency artifact present in the reconstructed signal has been removed by the deformation/interpolation operator. (b) from left to right: original fully sampled k-space data, undersampled data, k-space data of the reconstructed sequence and k-space data of the MC reconstructed sequence.

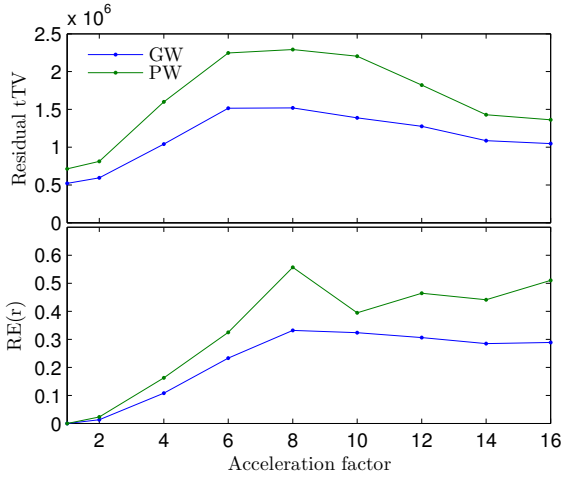

Figure 3: (top) Residual temporal Total Variation of the image after registration and (bottom) Registration Error (see Eq. 14) both for GW and PW approaches as a function of the acceleration factor.

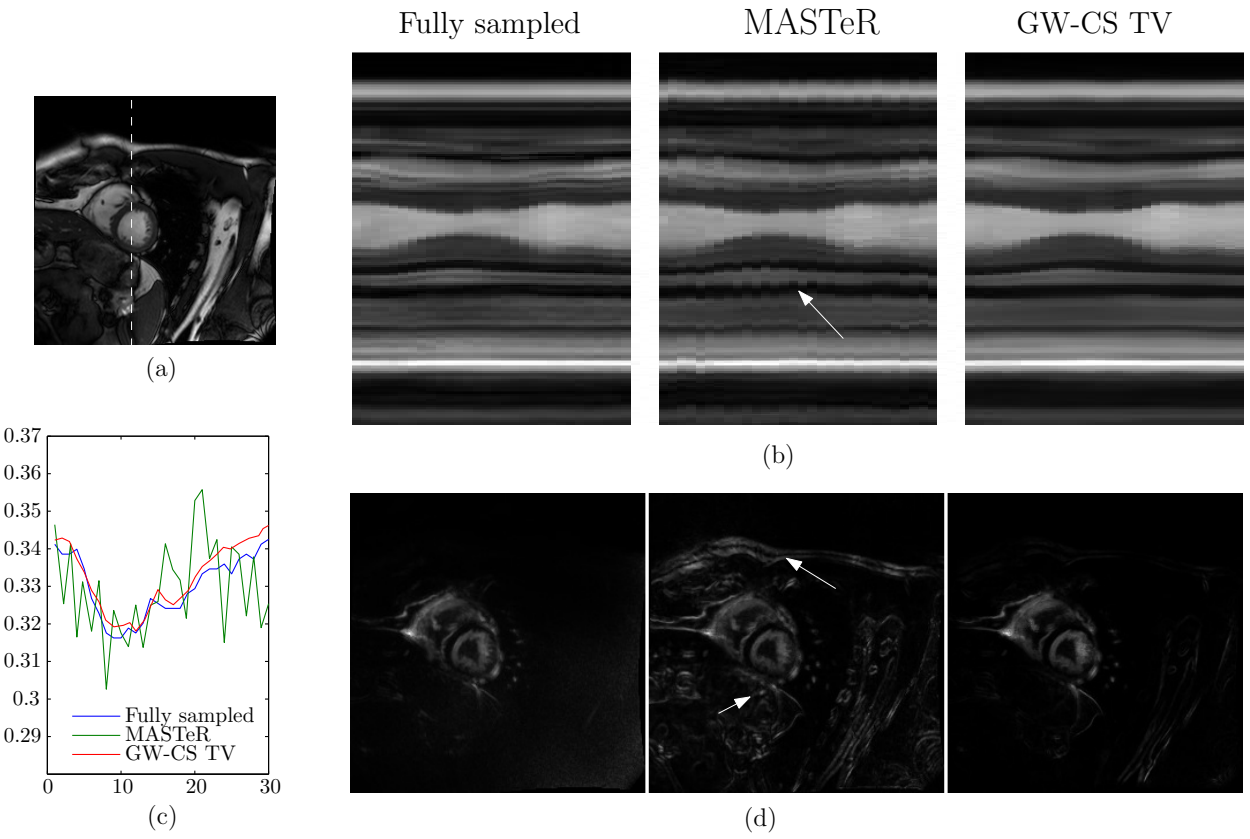

Figure 4: Effect of the corrupted ME on a short axis 10-fold undersampled cardiac cine sequence. (a) First frame of the original sequence. (b) Temporal evolution of the intensity profile at the location indicated in (a) by the dashed line. (c) Plot of intensity value along time of the pixel indicated by the arrow in (b), from the fully sampled and reconstructed sequences. (d) Temporal TV of original and final reconstructions.

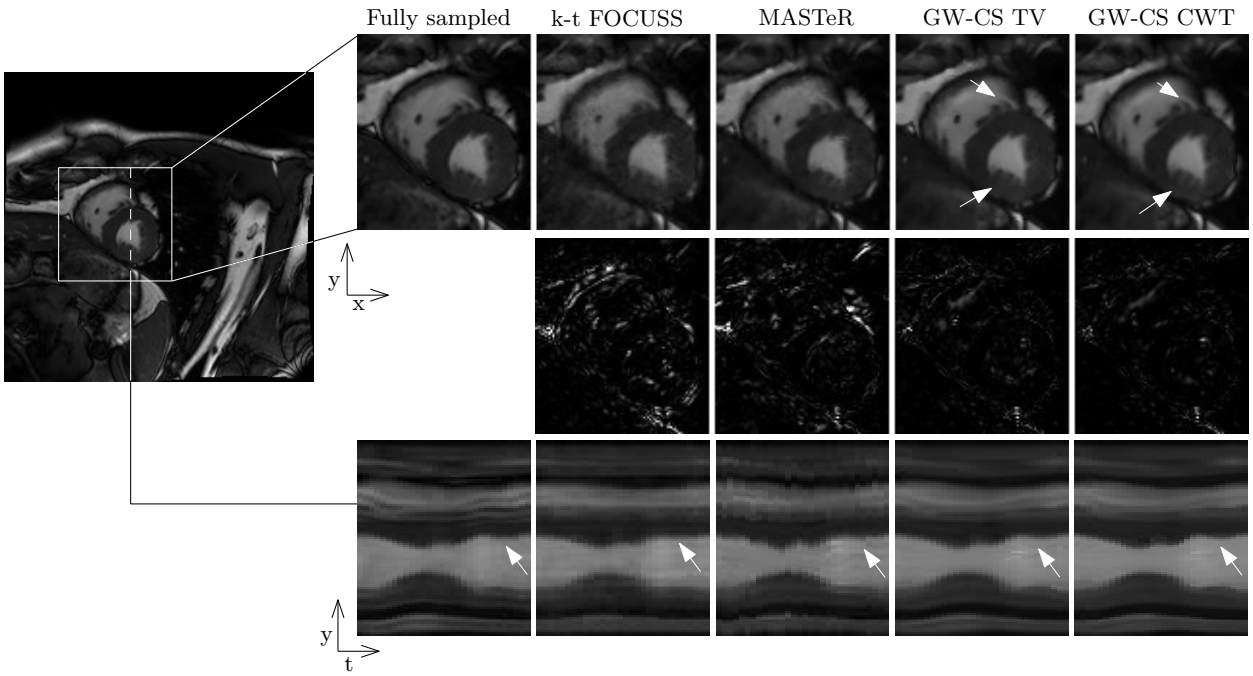

Figure 5: Short axis CINE reconstructions with the fully sampled data and k-t FOCUSS, MASTeR and the proposed GW-CS with TV and CWT as spatial sparsifying transforms with retrospective 12-fold undersampling. Single frame (top) and temporal evolution at the location indicated by dashed line (bottom). Middle row shows the absolute error of each image. Arrows in the bottom row indicate regions where fine motion detail has been lost in k-t FOCUSS.

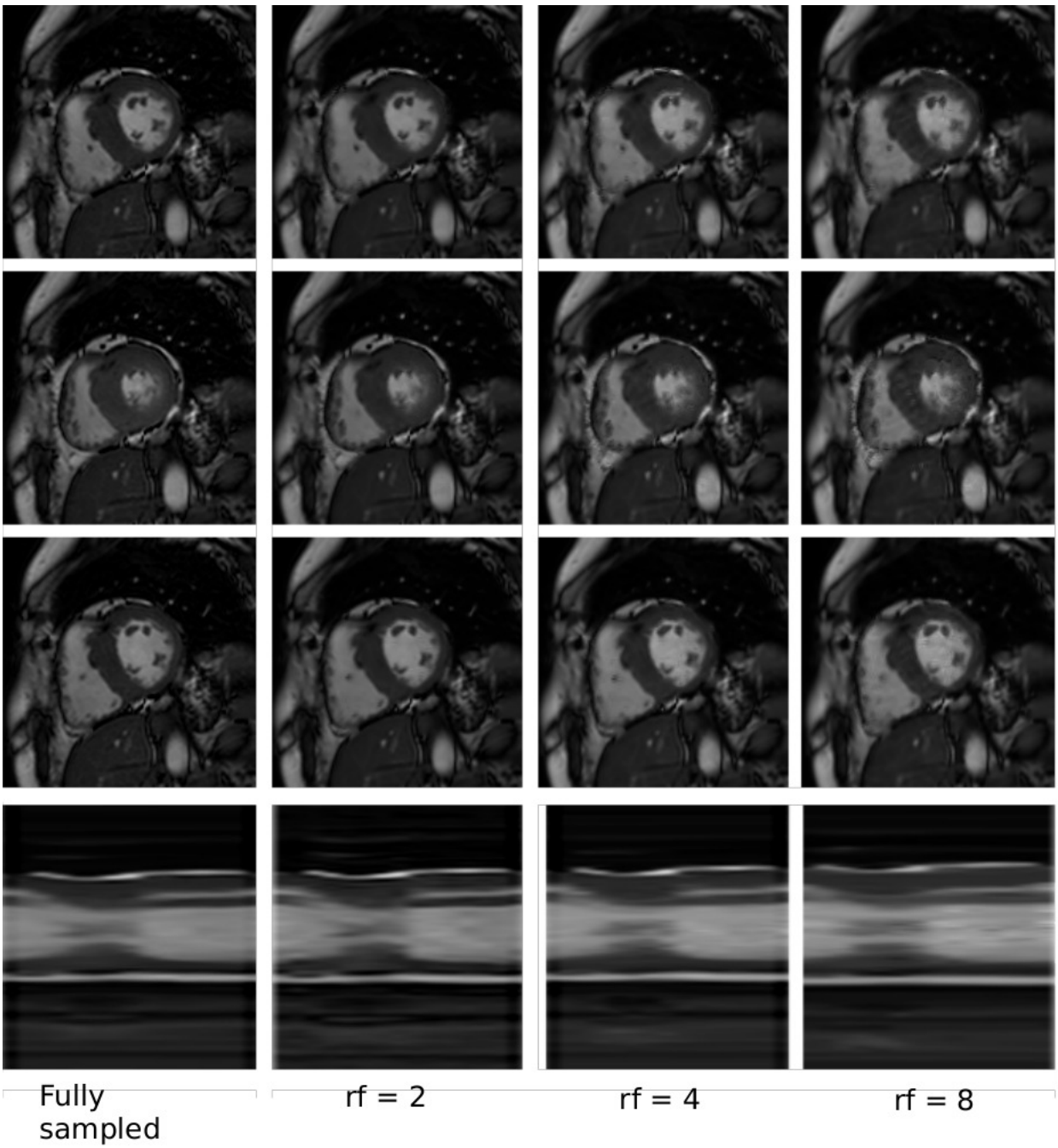

Figure 6: Reconstructions of the data from a patient with a diagnosed HCM for different values of the subsampling factor. As it can be observed, the most relevant information, is preserved in the final sequence. The last row in the figure represents the intensity profile of a vertical line taken at the center of the image. The intensity variation highlights that motion is preserved.

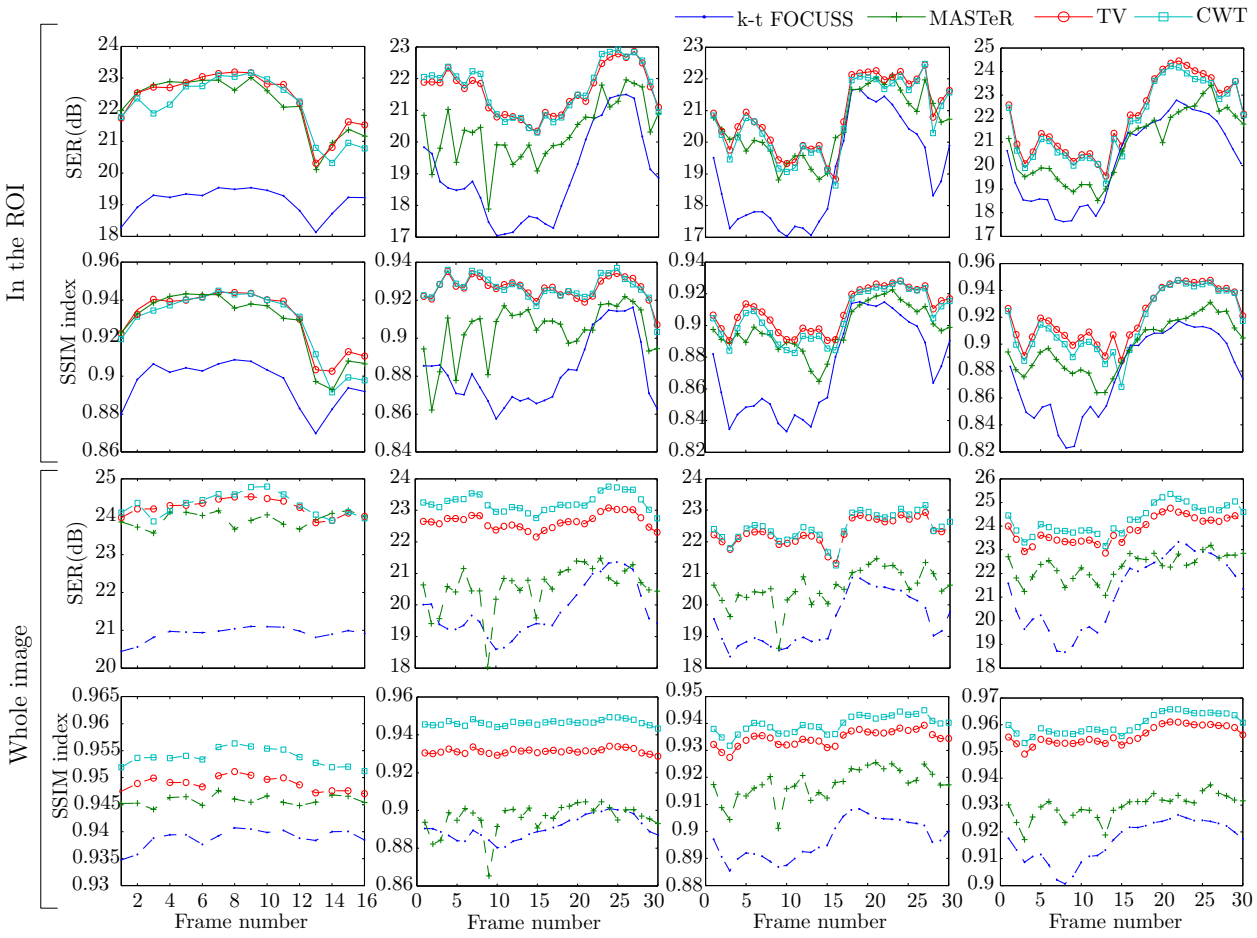

Figure 7: Quantitative quality measures for each frame on a 12-fold accelerated reconstruction of each dataset used. SER and SSIM index calculated over a ROI containing the heart and over the whole image. First column corresponds to the 1.5T data ad the remaining three columns to the 3T data.

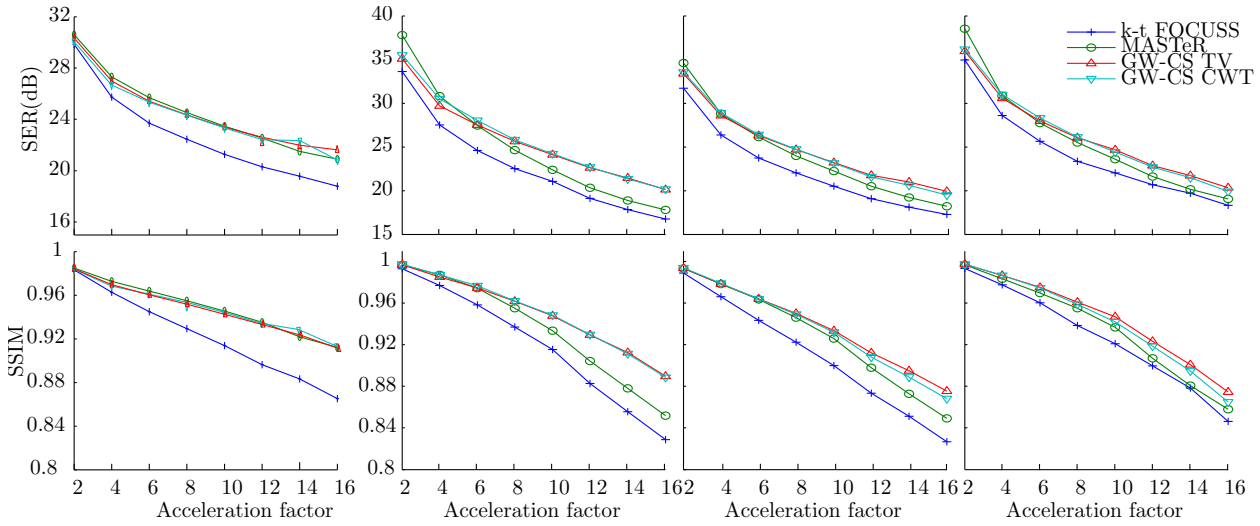

Figure 8: SER (top row) and SSIM index (bottom row) calculated over a ROI around the heart for the four reconstructed sequences. First columnn corresponds to 1.5T data and the remaining three columns to the 3T data.

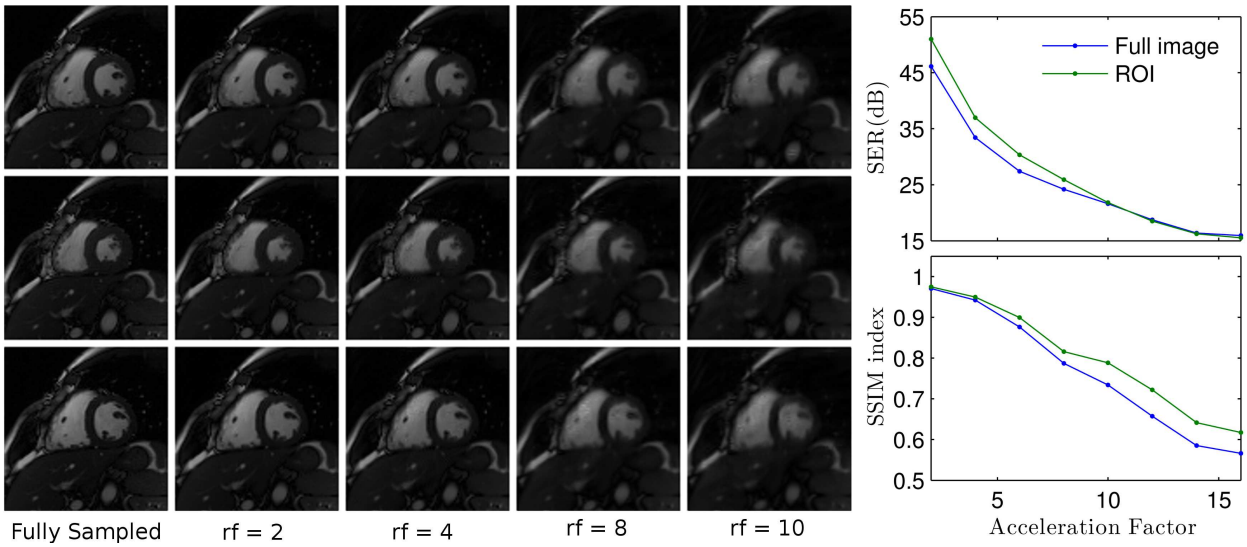

Figure 9: (left) Reconstruction of 32-coil acquisitions for different values of the acceleration factor; three instants of the cardiac cycle are shown from top to bottom; (right) SER and SSIM (in the whole image —blue— and within a ROI around the myocardium —green— as function of the acceleration factor for the images shown.